

TTR algorithm for the inversion of the exponential X-ray transform

J.-M. Wagner, F. Noo,
University of Liège, Belgium

Abstract

In this paper, we present an FBP algorithm suitable for image reconstruction from exponential X-ray projections sampled on any subset of the sphere that includes great circles. This algorithm is similar to the TTR-algorithm of Ra *et al.* (1982) for non-attenuated projections. It is derived by combining all reconstructions that can be obtained from the subsets of measurements corresponding to a great circle. Our results generalize those published by I. Hazou (1988) and Weng *et al.* (1996) for reconstruction from projections sampled on the unit sphere. However, they remain modest as they only apply to specific sets of measurements.

I. INTRODUCTION

This work presents new mathematical results concerning three-dimensional (3-D) image reconstruction from exponential X-ray (parallel-beam) projections.

The exponential X-ray transform is a mathematical tool useful in SPECT imaging and also in Intensity Modulated Radiation Therapy [1]. In 2-D SPECT, it is the basis for the development of fast analytical reconstruction methods with accurate correction for attenuation and depth-dependent collimator-response [2, 3]. In fully 3-D SPECT, it provides a way to perform accurate attenuation correction without transmission measurements [4], which is attractive for imaging systems such as the Rotating-Slant-Hole scanner [5].

2-D image reconstruction from exponential X-ray projections has been widely studied over the last twenty years and is now well-understood, especially thanks to the significant work of Pan and Metz [6, 7]. In fully 3-D geometry, the situation is quite different. To our knowledge, only two works concerning exact 3-D reconstruction from exponential X-ray projections have been published so far. These two works (see [8] and [9]) assume both that the projections are finely sampled on the unit sphere. It is currently unknown if exact reconstruction can be achieved from more general data sets, such as those satisfying Orlov's condition for reconstruction in the non-attenuated case [10]. Such a question is mathematically difficult to answer because 3-D reconstruction theory for non-attenuated X-ray projections [11] is not readily modified to handle exponential X-ray projections.

In this paper, we present a filtered-backprojection (FBP) algorithm suitable for image reconstruction from exponential X-ray projections sampled on any subset of the unit sphere that includes great circles. A basic example of such a subset is the equatorial band illustrated in figure 1a.

The derivation of our algorithm follows the same lines as the work of Ra *et al.* [12] for image reconstruction from non-attenuated projections. From the theory for the

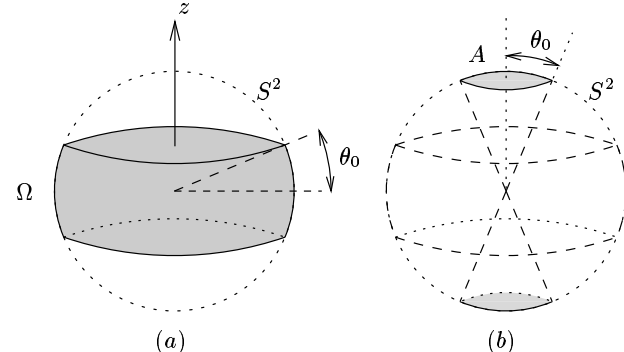


Figure 1: (a) Description of the equatorial band Ω (b) Description of the set A .

2-D Radon transform, Ra *et al.* derived the first True Three-dimensional Reconstruction (TTR) algorithm of FBP-type for non-attenuated X-ray projections. From the theory for the 2-D exponential Radon transform, we have derived an algorithm of FBP-type for 3-D image reconstruction from exponential X-ray projections. We call this new algorithm the A-TTR algorithm, where A stands for "attenuated".

Our results generalize those published by Hazou [8] and Weng *et al.* [9]. However, they remain modest as they only apply to specific sets of measurements on the unit sphere - those including great circles. We believe that our work is one step further towards full understanding of the 3-D exponential X-ray transform.

Section II gives a general description of the A-TTR algorithm. Section III concerns the application of the A-TTR algorithm to a particular geometry: the equatorial band. Conclusions are given in section IV.

II. A-TTR ALGORITHM

A. Notations

The data used for reconstruction are exponential X-ray projections

$$p(\underline{\theta}, \underline{s}) = \int_{-\infty}^{+\infty} dt f(\underline{s} + t \underline{\theta}) e^{\mu_0 t}, \quad \underline{s} \cdot \underline{\theta} = 0 \quad (1)$$

"measured" for a set of directions $\underline{\theta}$ on the unit sphere. The 3-D image to be reconstructed is f and μ_0 is the attenuation factor. Vector \underline{s} is orthogonal to $\underline{\theta}$ and is used to specify different lines of integration in the direction $\underline{\theta}$. See figure 2. We assume that the projections are complete, i.e. that $p(\underline{\theta}, \underline{s})$ is known for all \underline{s} orthogonal to $\underline{\theta}$.

Technically speaking, there exists no scanners which directly deliver exponential X-ray projections. However, to

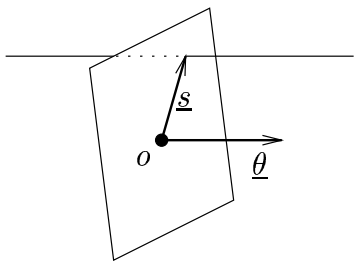


Figure 2: Description of the projections: \underline{s} is used to specify different lines of integration in the direction $\underline{\theta}$, O is the origin of the image space.

symplify the exposition we will assume that exponential X-ray projections can be directly measured.

If a detector with pixels of coordinates (u, v) oriented along unit orthogonal vectors $\underline{\alpha}$ and $\underline{\beta}$ perpendicular to $\underline{\theta}$ is used to measure $p(\underline{\theta}, \underline{s})$, one can write

$$\underline{s} = u \underline{\alpha} + v \underline{\beta}, \quad u \in \mathbb{R}, \quad v \in \mathbb{R} \quad (2)$$

$$p(\underline{\theta}, \underline{s}) = p_D(\underline{\theta}, u, v) = \int_{-\infty}^{+\infty} dt f(u \underline{\alpha} + v \underline{\beta} + t \underline{\theta}) e^{\mu_0 t}. \quad (3)$$

The set of directions $\underline{\theta}$ for which $p(\underline{\theta}, \underline{s})$ is known is denoted Ω . We assume that Ω is symmetric (i.e. if $\underline{\theta} \in \Omega$, then $-\underline{\theta} \in \Omega$) and contains great circles. A great circle is the set of unit vectors which are orthogonal to a given direction. We use the notation $C(\underline{n})$ to describe the great circle of unit vectors orthogonal to \underline{n} . The set of vectors \underline{n} corresponding to all great circles in Ω is denoted A . Note that A is symmetric. See figure 1b for an illustration of A for the equatorial band.

It is important to note that any great circle defines a complete set of projections from which exact reconstruction of f is possible. When Ω includes more than one great circle, the data $p(\underline{\theta}, \underline{s})$ are thus redundant.

B. Algorithm description

The A-TTR algorithm is an FBP algorithm which provides exact reconstruction of f according to the backprojection formula

$$f(\underline{x}) = \int_{\Omega} d\underline{\theta} e^{-\mu_0 \underline{x} \cdot \underline{\theta}} p^F(\underline{\theta}, \underline{x} - (\underline{x} \cdot \underline{\theta}) \underline{\theta}) \quad (4)$$

where $p^F(\underline{\theta}, \underline{s})$ is obtained from $p(\underline{\theta}, \underline{s})$ by 2-D convolution:

$$p^F(\underline{\theta}, \underline{s}) = \int_{\underline{s}' \cdot \underline{\theta}=0} d\underline{s}' p(\underline{\theta}, \underline{s} - \underline{s}') h(\underline{\theta}, \underline{s}'). \quad (5)$$

The convolution filter h is given by

$$h(\underline{\theta}, \underline{s}) = \begin{cases} 2c \frac{k_\mu(\|\underline{s}\|)}{\|\underline{s}\|} w(\underline{\theta} \times \frac{\underline{s}}{\|\underline{s}\|}) & \text{if } \underline{\theta} \times \frac{\underline{s}}{\|\underline{s}\|} \in A \\ 0 & \text{otherwise} \end{cases} \quad (6)$$

where the symbol \times denotes a cross product, w is some even positive function defined on the unit sphere ($w(-\underline{n}) = w(\underline{n})$),

$$c = 1 / \int_A d\underline{n} w(\underline{n}), \quad (7)$$

and k_μ is the notch filter used in FBP inversion of the 2-D exponential Radon transform:

$$k_\mu(r) = \int_{|\nu|>\mu_0/2\pi} d\nu \frac{|\nu|}{2} e^{j2\pi r\nu}. \quad (8)$$

As readily observed from its definition, the filter h is a generalized function with singularities at $\underline{s} = 0$. Equation (5) for $p^F(\underline{\theta}, \underline{s})$ should thus be interpreted as a Cauchy principal value. For numerical computation of $p^F(\underline{\theta}, \underline{s})$, it is preferable to implement (5) in the Fourier domain. The frequency expression of the filter required for this implementation is

$$\begin{aligned} H(\underline{\theta}, \underline{\nu}) &= \int_{\underline{s} \cdot \underline{\theta}=0} d\underline{s} e^{-j2\pi \underline{s} \cdot \underline{\nu}} h(\underline{\theta}, \underline{s}) \\ &= \frac{c}{2} \int_{C^*(\underline{\theta}) \cap A} d\underline{n} w(\underline{n}) |\underline{\nu} \cdot (\underline{n} \times \underline{\theta})|, \quad \underline{\nu} \cdot \underline{\theta} = 0 \end{aligned} \quad (9)$$

where $C^*(\underline{\theta})$ is a subset of the great circle $C(\underline{\theta})$:

$$C^*(\underline{\theta}) = C(\underline{\theta}) \setminus \{\underline{n} \in C(\underline{\theta}) : |\underline{\nu} \cdot (\underline{n} \times \underline{\theta})| < \mu_0/2\pi\}. \quad (10)$$

Note, in particular, that $C^*(\underline{\theta}) = \emptyset$ when $\|\underline{\nu}\| < \mu_0/2\pi$ because $|\underline{\nu} \cdot (\underline{n} \times \underline{\theta})| < \mu_0/2\pi$ for any \underline{n} in this case. Therefore,

$$H(\underline{\theta}, \underline{\nu}) = 0 \quad \text{if } \|\underline{\nu}\| < \mu_0/2\pi. \quad (11)$$

III. APPLICATION: EQUATORIAL BAND

In this section, we apply the A-TTR algorithm to the equatorial band. No FBP algorithm had been published so far for the equatorial band geometry.

Thus, here, Ω is the equatorial band of aperture θ_0 illustrated in figure 1a. Mathematically, we write

$$\Omega = \left\{ \underline{\theta} \in S^2 : |\underline{\theta} \cdot \underline{e}_z| \leq \sin \theta_0 \right\}. \quad (12)$$

For this set, one has

$$A = \left\{ \underline{n} \in S^2 : |\underline{n} \cdot \underline{e}_z| \geq \cos \theta_0 \right\}. \quad (13)$$

See figure 1b. Equation (13) with (6) specifies the spatial-domain expression of the A-TTR filter. Below, we give details on the calculation of the frequency-domain expression of the filter. For this calculation, $w(\underline{n}) = 1$ is assumed. That is

$$c = \frac{1}{4\pi (1 - \cos \theta_0)} \quad (14)$$

(see equation (7)). Recall first that $H(\underline{\theta}, \underline{\nu}) = 0$ when $\|\underline{\nu}\| < \mu_0/2\pi$, i.e. $H(\underline{\theta}, \underline{\nu})$ needs only to be calculated for $\|\underline{\nu}\| \geq \mu_0/2\pi$. We introduce unit orthogonal vectors $\underline{\alpha}$ and $\underline{\beta}$ such that $\underline{\alpha} \times \underline{\beta} = \underline{\theta}$. We also define angles ω and ψ such that

$$\begin{aligned} \underline{n} &= \cos \omega \underline{\alpha} + \sin \omega \underline{\beta}, \\ \underline{n} \times \underline{\theta} &= \sin \omega \underline{\alpha} - \cos \omega \underline{\beta}, \\ \underline{\nu} &= \|\underline{\nu}\| (\cos \psi \underline{\alpha} + \sin \psi \underline{\beta}). \end{aligned} \quad (15)$$

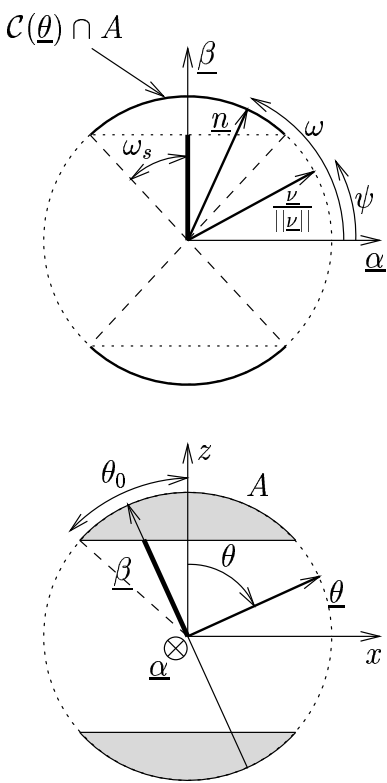


Figure 3: Top: Description of $\mathcal{C}(\underline{\theta}) \cap A$. Bottom: Intersection of the unit sphere with the plane $(\underline{\theta}, \underline{\beta})$. In both figures the dark segment of line has the same length. Expressing that condition leads to equation (20) for ω_s .

With these notations, one has

$$\underline{\nu} \cdot (\underline{n} \times \underline{\theta}) = \|\underline{\nu}\| \sin(\omega - \psi) \quad (16)$$

$$\mathcal{C}^*(\underline{\theta}) = \left\{ \underline{n} = \cos \omega \underline{\alpha} + \sin \omega \underline{\beta} : |\sin(\omega - \psi)| > \sin \omega_m \right\}. \quad (17)$$

where

$$\sin \omega_m = \frac{\mu_0}{2\pi \|\underline{\nu}\|}. \quad (18)$$

To carry out the calculation of $H(\underline{\theta}, \underline{\nu})$ according to formulas (9) and (10), note that

$$\mathcal{C}^*(\underline{\theta}) \cap A = \mathcal{C}^*(\underline{\theta}) \cap (\mathcal{C}(\underline{\theta}) \cap A). \quad (19)$$

Figure 3(top) illustrates the region $\mathcal{C}(\underline{\theta}) \cap A$. This region consists of two arcs of aperture $2\omega_s$ diametrically opposed. It is convenient to select the vectors $\underline{\alpha}$ and $\underline{\beta}$ to be the symmetry axes of $\mathcal{C}(\underline{\theta}) \cap A$ as shown in figure 3(top). The angle ω_s is defined by

$$\cos \omega_s = \frac{\cos \theta_0}{\sin \theta} \quad (20)$$

where θ is the polar angle of $\underline{\theta}$. See figure 3(bottom). Mathematically, one has

$$\mathcal{C}(\underline{\theta}) \cap A = \left\{ \underline{n} = \cos \omega \underline{\alpha} + \sin \omega \underline{\beta} : |\sin \omega| > \cos \omega_s \right\}. \quad (21)$$

Therefore, involving equations (16), (17) and (21), one finds

$$H(\underline{\theta}, \underline{\nu}) = \frac{\|\underline{\nu}\|}{8\pi(1 - \cos \theta_0)} \int_W d\omega |\sin(\omega - \psi)| \quad (22)$$

where

$$W = \left\{ \omega \in [0, 2\pi[: \begin{array}{l} |\sin(\omega - \psi)| \geq \sin \omega_m, \\ |\sin \omega| > \cos \omega_s \end{array} \right\}. \quad (23)$$

From these two last equations, one can easily check that $H(\underline{\theta}, \underline{\nu})$ needs only to be known for $\psi \in [0, \pi/2[$ because replacing ψ by $-\psi$ or $\psi + \pi$ does not change the filter expression. Straightforward (but tedious) calculation of the integral in (22) leads to the expression given in table 1 for $H(\underline{\theta}, \underline{\nu})$.

Note that the filter $H(\underline{\theta}, \underline{\nu})$ is here identical for directions $\underline{\theta}$ which have the same polar angle θ but different azimuthal angles. This is because $w(\underline{n}) = 1$ was selected and Ω is symmetric about the z -axis. Figure 4 shows the look of $H(\underline{\theta}, \underline{\nu})$ for $\theta = 90^\circ$ and $\theta = 46^\circ$ respectively, when $\theta_0 = 45^\circ$. Only the part $\psi \in [0, \pi/2[$ is displayed.

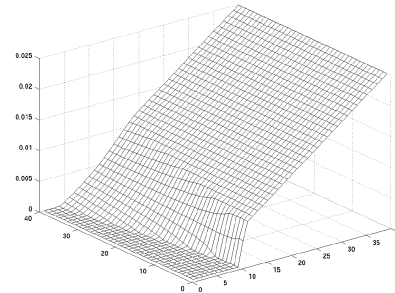
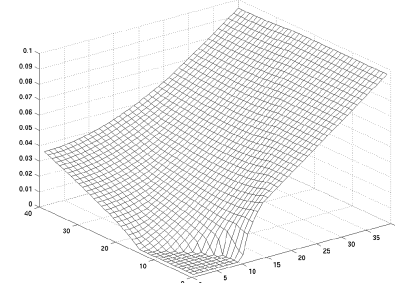


Figure 4: Frequency-domain filter for the equatorial band - Top: $\theta = 90^\circ$. Bottom: $\theta = 46^\circ$.

Figure 4 shows the reconstruction of a simulated phantom modelling the heart. This phantom consists of three ellipsoids, two of which model the ventricles with 20% of activity. The reconstruction was achieved on a grid of 100^3 cubic voxels of side 1.5 mm, using $\theta_0 = 45^\circ$ and $\mu_0 = 0.0152 \text{ mm}^{-1}$. The set Ω was uniformly sampled in spherical coordinates with a step of 3 degrees and the projections were sampled on grids of 128^2 pixels of side 1.5 mm. The quality of the reconstruction in figure 5 demonstrates the exactness of the algorithm.

IV. CONCLUSIONS

We have developed an FBP algorithm for exact 3-D image reconstruction from exponential X-ray projections sampled on any subset of the unit sphere that includes great circles. The A-TTR algorithm generalizes all previously published results [8, 9]. However, our findings remain modest as it only applies

$G(\psi, \omega_m)$		$\omega_m < \omega_s$	$\omega_m \geq \omega_s$
$\psi < \frac{\pi}{2} - \omega_s - \omega_m$	$\frac{\pi}{2} + \psi_s < \pi + \psi - \omega_m$ $\frac{\pi}{2} + \psi_s \geq \pi + \psi - \omega_m$	$4 \sin \psi_s \cos \psi$ $2 \cos \omega_m + 2 \sin \omega_s \cos \psi + 2 \sin \psi \cos \omega_s$	
$\frac{\pi}{2} - \omega_s - \omega_m \leq \psi < \frac{\pi}{2} - \omega_s - \omega_m $	$\frac{\pi}{2} + \omega_s < \pi + \psi - \omega_m$ $\frac{\pi}{2} + \omega_s \geq \pi + \psi - \omega_m$	$2 \cos \omega_m + 2 \sin \omega_s \cos \psi - 2 \sin \psi \cos \omega_s$ $4 \cos \omega_m$	
$\frac{\pi}{2} - \omega_s - \omega_m \leq \psi < \frac{\pi}{2}$		$4 \cos \omega_m - 4 \sin \psi \cos \psi_s$	0

Table 1

Frequency-domain expression of the A-TTR filter for the equatorial band. The filter is expressed in the form $H(\underline{\theta}, \underline{\nu}) = G(\psi, \omega_m) \|\underline{\nu}\| / 8\pi(1 - \cos \theta_0)$. The table gives the values of $G(\psi, \omega_m)$ according to the values taken by ψ , ω_s and ω_m . The vector $\underline{\nu} = \|\underline{\nu}\| (\cos \psi \underline{\alpha} + \sin \psi \underline{\beta})$. The table should only be used for $\psi \in [0, \pi/2]$ and $\|\underline{\nu}\| \geq \mu_0/2\pi$. For $\|\underline{\nu}\| < \mu_0/2\pi$, $H(\underline{\theta}, \underline{\nu}) = 0$. The dependence of $H(\underline{\theta}, \underline{\nu})$ on $\underline{\theta}$ is buried in the definition of ω_s (see equation (20)).

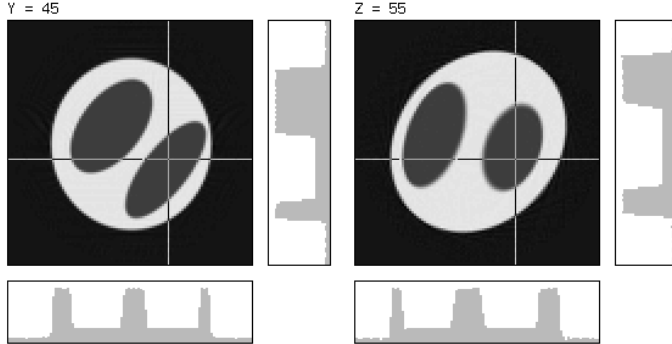


Figure 5: Equatorial band. Reconstruction of a simulated phantom of the heart for $\theta_0 = 45$ degrees and $\mu_0 = 0.0152 \text{ mm}^{-1}$. Left: vertical slice. Right: horizontal slice.

to particular set of projections - those containing great circles. Further investigations are required for reconstruction from more general data sets.

ACKNOWLEDGEMENTS

The work of F. Noo was supported by the Belgian National Fund for Scientific Research. The authors thank M. Defrise for fruitful discussions on the topic of this paper.

V. REFERENCES

- [1] M. Braunstein, R.Y. Levine, "Optimum beam configurations in tomographic intensity modulated radiation therapy", *Phys. Med. Biol.*, Vol. 45, 305-328, 2000.
- [2] S. J Glick, B. C. Penney, M. A. King, and C. L. Byrne, "Noniterative compensation for the distance-dependent detector response and photon attenuation in SPECT imaging", *IEEE Trans. Med. Imag.*, vol. 13(2), 363-374, 1994.
- [3] X. Pan and C. E. Metz, "Analytical approaches for image reconstruction in 3D SPECT", in *Three-dimensional Image Reconstruction in Radiation and Nuclear Medicine*, ed. P. Grangeat and J.-L. Amans (Dordrecht: Kluwer), 103-115, 1996.
- [4] C. Mennessier, F. Noo, R. Clack, G. Bal, L. Desbat, "Attenuation correction in SPECT using consistency conditions for the exponential ray transform", *Phys. Med. Biol.*, Vol 44, 2483-2510, 1999.
- [5] R. Clack, P.E. Christian, M. Defrise, A.E. Welch, "Image reconstruction for a novel SPECT system with rotating slant-hole collimators". In *Conf. Rec. 1995 IEEE Med. Imag. Conf.*, 1948-1952, 1996.
- [6] C.E. Metz, X. Pan, "A unified analysis of exact methods of inverting the 2D exponential Radon transform, with implications for Noise Control in SPECT", *IEEE Trans. Med. Imag.*, vol. 14(4), december 1995.
- [7] X. Pan, C.E. Metz, "Analysis of noise properties of a class of exact methods of inverting the 2D exponential Radon transform", *IEEE Trans. Med. Imag.*, vol. 14(4), december 1995.
- [8] I.A. Hazou, "Inversion of the exponential X-ray transform. I: Analysis", *Math. Methods in the Applied Sciences*, Vol. 10(10), 561-574 (1988).
- [9] Y. Weng, G.L. Zeng, G.T. Gullberg, "Filtered backprojection algorithms for attenuated parallel and cone-beam projections sampled on a sphere", in *Three-dimensional Image Reconstruction in Radiation and Nuclear Medicine*, ed. P. Grangeat and J.-L. Amans (Dordrecht: Kluwer), 19-34, 1996.
- [10] S.S. Orlov, "Theory of three dimensional reconstruction. 1. Conditions of a complete set of projections.", *Sov. Phys.-Crystallogr.*, Vol. 20, 312-314, 1975.
- [11] M. Defrise, D.W. Townsend, R. Clack, "Three-dimensional image reconstruction from complete projections", *Phys. Med. Biol.*, Vol. 34(5), 573-587, 1989.
- [12] J. B. Ra, C. B. Lim, Z.H. Cho, S.K. Hilal, J. Correll "A true three-dimensional reconstruction algorithm for the spherical positron emission tomograph", *Phys. Med. Biol.* Vol. 27, 37-50, 1982.
- [13] O. Tretiak, C. Metz, "The exponential Radon transform", *SIAM J. Appl. Math.*, Vol. 39(2), 341-354, 1980.